

Quantitative prediction model for affinity of drug-target interactions based on molecular vibrations and overall system of ligand-receptor

Z. H. Zheng^a, Y. K. Liu^b, Y. Pei^a, J. Zhang^a, Z. W. Wang^b, H. Y. Wei^c, Z. G. Wu^{a,*}, J. W. Li^b

^aCollege of pharmacy, North China University of Science and Technology, Tangshan 063210, Hebei, People's Republic of China

^bInstitute of Oncology, Tangshan People's Hospital, Tangshan 063001, Hebei, People's Republic of China

^cCollege of Material Science and Engineering, North China University of Science and Technology, Tangshan 063210, Hebei, People's Republic of China

Herein, surface-enhanced Raman scattering (SERS) and ultraviolet visible absorption spectrum in combination with fluorescence spectroscopy were jointly explored to investigate the binding interaction between Enrofloxacin (EFLX) with Bovine serum albumin (BSA) at a physiological condition. A facile SERS substrate based on the self-assembly of colloid silver on the modified TiN-Ag surface was obtained, an advanced SERS analysis method basing on this as-prepared substrate was established for sensitive and rapid detection of enrofloxacin, the most enhanced mode was that with certain motions perpendicular to the metal surface. In addition, the fluorescence and ultraviolet spectrum were allowed to found that enrofloxacin may bind to BSA site I via the carboxyl group with strong binding power.

(Received July 3, 2023; Accepted August 14, 2023)

Keywords: Enrofloxacin, Bovine serum albumin, Binding interaction

1. Introduction

Enrofloxacin (EFLX), which belongs to the fluoroquinolone group of drugs, has been found to inhibit most gram-negative pathogens, including the *pseudomonas aeruginosa* and *enterobacteriaceae*. In medical aspects, it can be used for respiratory infections, gonorrhoea, bacterial gastroenteritis, skin soft tissue infections, uncomplicated and complicated urinary tract infections, especially those caused by Gram-negative and Gram-positive^[1]. As one of the most abundant proteins in the circulatory system, serum albumins are the major transport protein in blood and can reversibly bind to small molecules like fatty acids, amino acids, drugs, and inorganic ions^[2]. For example, human serum albumin (HSA) contains 585 amino acid residues, and it serves as an important carrier for many substances such as fatty acids, bilirubins, hormones, and exogenous or endogenous ligands. X-ray crystallographic analysis of HSA has revealed that this

* Corresponding author: 3229219366@qq.com

globular protein consists of three homologous alpha-helical domains (I-III), each of which is subdivided into two subdomains A and B^[3-4]. Moreover, Bovine serum albumin (BSA) is not only widely used in biomedical and pharmaceutical applications, but also widely utilized as a ligand-biological model to study the interactions between small molecules and globular proteins, due to its high stability, low-cost, versatile ligand-binding properties, medical significance and high structural homology with human serum albumin (HSA) (approximately 76%)^[5].

Hence, BSA has attracted much attention as an alternative model for HSA^[6]. Competitive studies and crystal structure analysis enabled the identification of specific ligand binding site within the hydrophobic cavities of the protein template named either subdomains IIA or Sudlow's site I respectively, and the tryptophan (Trp 134, Trp213) residue in BSA are located in Sudlow I.

After several decades of development since it was discovered on electrochemically roughened silver in 1973, surface-enhanced Raman scattering (SERS) has become a powerful analytical tool for applications of chemical and biological molecule detection, environmental monitoring, and food safety^[7-8]. For the rapid development of SERS technology, the successful fabrication of various SERS-active substrates plays one of the most significant roles^[9]. Generally, an important condition for the generation of the SERS effect is the synthesis of rough metal surfaces, mostly using noble metals such as gold, silver, and copper as active substrates because of their excellent electron transport capabilities. However, there are some disadvantages to use noble metals for working as SERS substrates, such as high cost, poor uniformity, lack of stability, and biocompatibility, side-reactions of the adsorbate due to the catalytic effect of metals, which seriously restrict the utilization of noble-metal SERS substrates in practical applications^[10-11]. In recent years, it is found that the titanium nitride (TiN) thin films have been extensively used in a wide range of applications as wear-protective coatings on mechanical components, cutting tools, decorations, as well as diffusion barriers and metal gates in integrated circuits, owing to its remarkable physical and chemical properties such as high hardness, high thermal stability, low electrical resistivity, and high wear excellent corrosion resistance^[12-16].

In the present study, a new method based on fluorescence, UV-visible absorption, Raman spectroscopy and surface-enhanced Raman spectroscopy in combination with highly site-competitive labelling experiments was jointly used to predict the affinity of drug-target interactions and obtain the molecular vibration model of EFLX with BSA.

2. Experimental

2.1. Materials

Anhydrous ethanol (C₂H₅OH, AR), titanium tetrachloride (TiCl₄, AR), polyvinylpyrrolidone (PVP, Mw=1300000, AR), N,N-dimethylformamide (DMF, AR), silver nitrate (AR, AgNO₃), trisodium citrate (AR, Na₃C₆H₅O₇·H₂O), enrofloxacin, ibuprofen, butazone, digoxin (purity > 98%) were purchased from Aladdin Reagents Ltd. Bovine serum albumin and Tris-HCl buffer (1 mol/L, pH 7.4) were purchased from Solebro Reagents Ltd. Bovine serum albumin solution (BSA): 0.665 g BSA, dissolved in Tris-HCl buffer to obtain a BSA solution at a concentration of 1.0 × 10⁻⁴ mol/L, stored at 4°C in a refrigerator.

2.2. Preparation of TiN-Ag/silver sol thin films

The precursor solution was prepared as follows: 0.5 ml of TiCl_4 was carefully mixed with 5.5 ml of anhydrous ethanol, and then 1.0 g of PVP was added. Ten milliliters of anhydrous ethanol and 2.5 ml of DMF were subsequently added in the solution to enhance the dissolution of PVP. The solution was magnetic stirred at room temperature for 3 h until the PVP was completely dissolved.

The quartz glass substrates were cleaned with deionized water and ethanol in an ultrasound bath. The thin films were deposited on the substrates by spin coating the precursor solution at 3500 rpm for 20 s. After drying at 80 °C in an oven for 24 h, the coated substrates were calcined at 600 °C in air for 0.5 h with a heating rate of 5 °C/min to remove PVP and obtain TiO_2 thin films.

The TiO_2 thin films were subsequently nitrated under NH_3 gas flow in a quartz tube furnace with a heating rate of 5 °C/min to different temperatures (600 °C to 1100 °C) for 2 h. The quartz tube was evacuated and flushed with N_2 gas for 0.5 h before heating. As the heating temperature increased up to 300 °C, the N_2 gas was replaced by NH_3 gas. The flow rate of NH_3 gas was kept about 400 ml/min from 300 °C to 500 °C. When the nitridation temperature reached to 500 °C, the flow rate of NH_3 gas was adjusted to 800 ml/min. The samples were cooled under NH_3 gas until the furnace temperature decreased to 300 °C, then N_2 gas was used instead of NH_3 gas.

The AgNO_3 solution was obtained as follows: 0.0169 g of silver nitrate was dissolved in 20 mL of deionised water, and the deposition solution with a silver nitrate concentration of 5 mmol/L was obtained after ultrasonic shaking. The TiN-Ag thin films were prepared via using a TiN film substrate as the working electrode, a Pt sheet as the counter electrode, a voltage of 5 V and a deposition time of 5 min.

The silver sol solution was received as follows: 0.018 g of silver nitrate was dissolved in 100 mL of deionised water, and then heat in a water bath until boiling. After the temperature reached at 100 °C, 2 mL of 0.01 g/mL sodium citrate was dropwise added and the reaction continued for 1 h to acquire a yellow-green silver solution, and then the silver sol solution was centrifuged under 8000 rpm for 10 minutes. The TiN-Ag/silver sol substrate was obtained via aspirating and dropping the lower layer solution onto the surface of the TiN-Ag membrane.

2.3. Characterization of TiN-Ag/silver thin films

The surface morphology of TiN-Ag/silver thin film was observed through scanning electron microscopy (SEM, JSM-7900F, JEOL), both of which are equipped with energy dispersive spectrometer (EDS) analyzer.

2.4. SERS detection

The enrofloxacin was dissolved in pH 7.4, 0.01 mol/L Tris-HCl buffer and BSA to obtain the enrofloxacin-BSA complexes solution. All solutions were mixed with silver sol (1:1,v/v) and dropped onto the TiN-Ag/silver sol substrate surface for detection. The Raman spectra of the samples were recorded on Raman microscopic spectrometer (DXR, Thermo Fisher). A 780-nm laser with the power of 15.0 mW was used as the excitation source. The laser beam was focused on the sample surface through a 10×microscope objective. The collection time of a single Raman

spectrum was 10 s. The Raman spectra of all samples were obtained by measuring different spots in the samples.

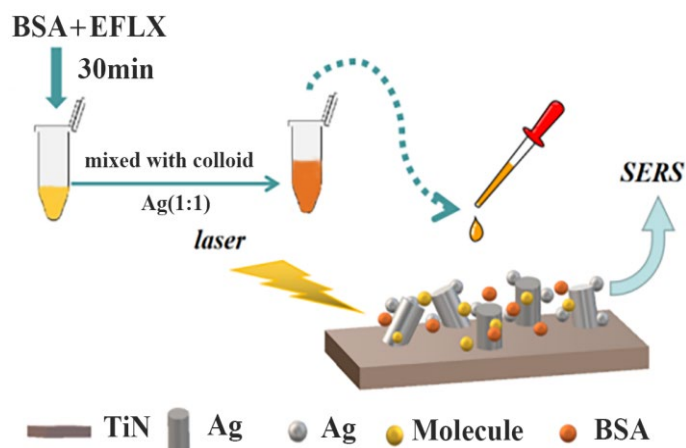


Fig. 1. Diagram of SERS experimental procedure.

2.4. UV-Vis spectroscopy testing

The Enrofloxacin-BSA complexes solution was diluted in Tris-HCl buffer to obtain the solution of $(1,3,5,7) \times 10^{-5}$ mol/L. The UV-Vis spectrum of various densities was measured by UV-Vis spectrophotometer (Lambda 750S, Perkin Elmer).

2.5. Fluorescence studies

Temperature variation experiments: The enrofloxacin and BSA were incubated in a water bath at 298 K and 310 K respectively for 30 minutes and then immediately removed for fluorescence detection. Site competition experiments: The phenylbutazone, ibuprofen and digoxin were all dissolved in anhydrous ethanol and diluted with deionised water to obtain the labelling reagents with a concentration of 2×10^{-4} mol / L. Field competition experiments: BSA was first mixed with the labelling reagents at 298 K, and then enrofloxacin was added carefully. In subsequent experiments, all solutions were diluted with pH 7.4, 0.01 mol/L Tris-HCl buffer. The spectra of the solutions were conducted with fluorescence spectrophotometer (RF-5301PC, Shimadzu, Japan). An excitation wavelength of 295 nm was chosen and the emission wavelength range was 300-500 nm. The widths of the excitation slit and emission slit were set to 3 nm and 1.5 nm, respectively.

3. Results and discussion

3.1. The characterization of TiN-Ag/silver thin films

As depicted in Figure 2, scanning electron microscopy (SEM) was utilized to examine the surface topography and morphology of all prepared TiN-Ag/silver thin films. As displayed in Fig.2(a,b), a uniform TiN layer covering a large number of tetragonal Ag spheres can be well-distinguished. To further visualize the distribution of titanium nitride and silver, the

Energy-dispersive spectroscopy (EDS)-based elemental mapping was conducted (Fig.2c). Furthermore, scanning transmission electron microscopic high-angle annular dark field imaging and corresponding elemental mapping (Fig. 2d,e,f) show the uniform distributions of Ag, Ti and N elements, although there is a spreading of N and Ti elements in the image. The SEM and EDS analysis illustrate that Ti, N and Ag elements are distributed on the surface of composite film, further confirming the existence of titanium nitride and silver nanoparticles.

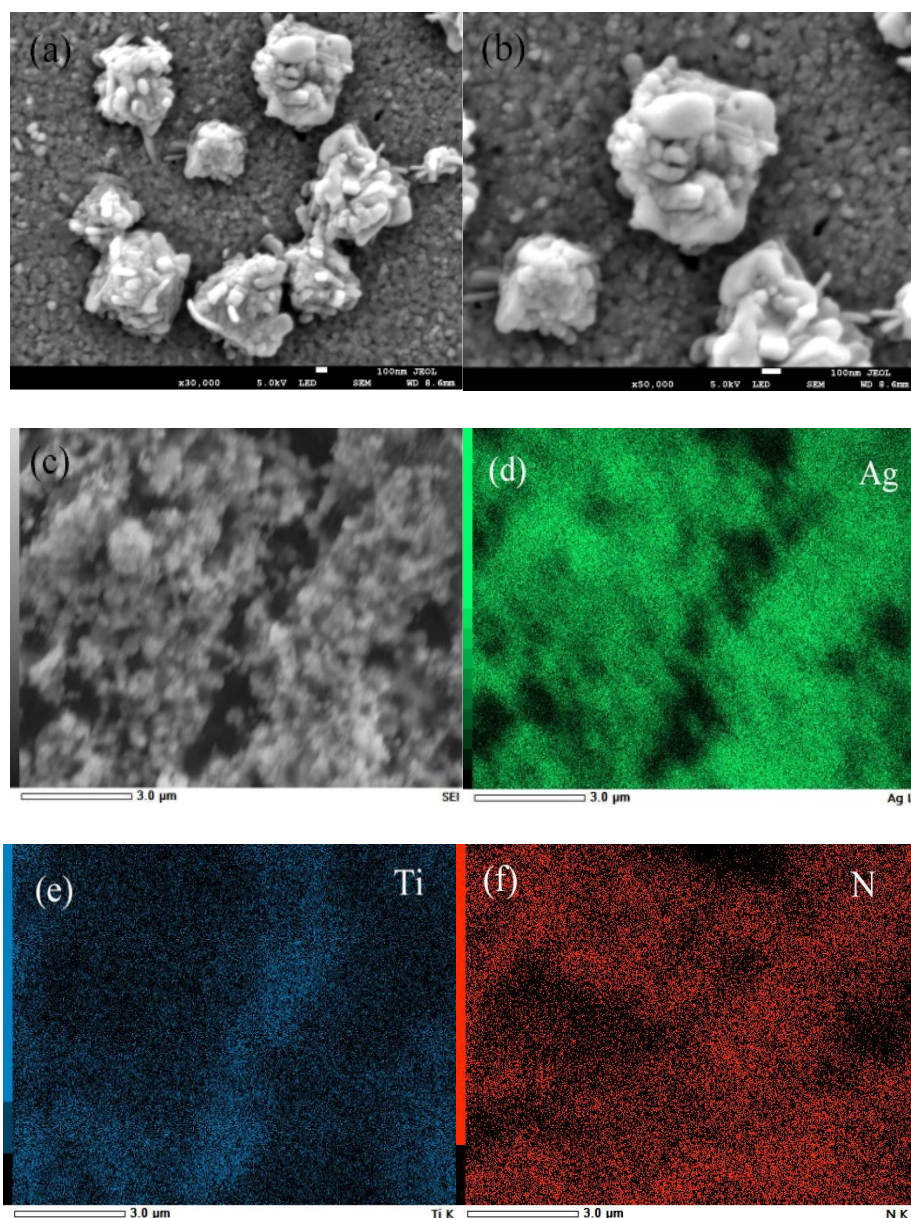


Fig. 2. (a)~(b) SEM images of TiN-Ag@silver composite substrate, (c)~(f) Dark-field images of another individual TiN-Ag@silver sphere and the corresponding elemental mapping of Ag, Ti, and N.

3.2. Enrofloxacin-BSA interactions combined for NR and SERS spectroscopy

As can be depicted in Fig.3A, the normal Raman spectroscopy obtained from the solid enrofloxacin was dominated by a band at 1381 cm^{-1} which can be mainly attributed to the OC=O

stretching vibration mode, as well as the band at 725 cm^{-1} which was primarily assigned to the methylene ($-\text{CH}_2$) oscillation vibration mode. Moreover, the band around 1608 cm^{-1} was likely the $\text{C}=\text{O}$ stretching vibration mode. The peaks observed at 725 and 1381 cm^{-1} were slightly enhanced and shifted to 745 and 1382 cm^{-1} in the SERS spectrum, respectively. However, the peak at 1608 cm^{-1} had a remarkable blue shift to that of the 1600 cm^{-1} SERS signal^[17-19].

Fig.3B revealed the SERS spectra of different concentrations of EFLX-BSA complexes solution dispersed onto the TiN-Ag/silver sol substrates surface. All the measurements were conducted under identical experiment conditions (incubation duration, laser power, acquisition time). From the concentration-dependent SERS spectra shown in Figure 3B, we found that the intensity of the vibrations at 745 cm^{-1} , 1382 cm^{-1} , 1600 cm^{-1} enhanced greatly when the concentration of EFLX increased from $1 \times 10^{-2}\text{ M}$ to $4 \times 10^{-2}\text{ M}$ after the interaction with BSA. Hence, these results suggested that negatively charged groups, mainly carboxyl groups, on the BSA molecule interacted with the EFLX surface. According to the surface selection principle^[20-21], it can be judged that the adsorption mode of EFLX on the metal surface gradually tended to be vertical with the increase of EFLX concentration.

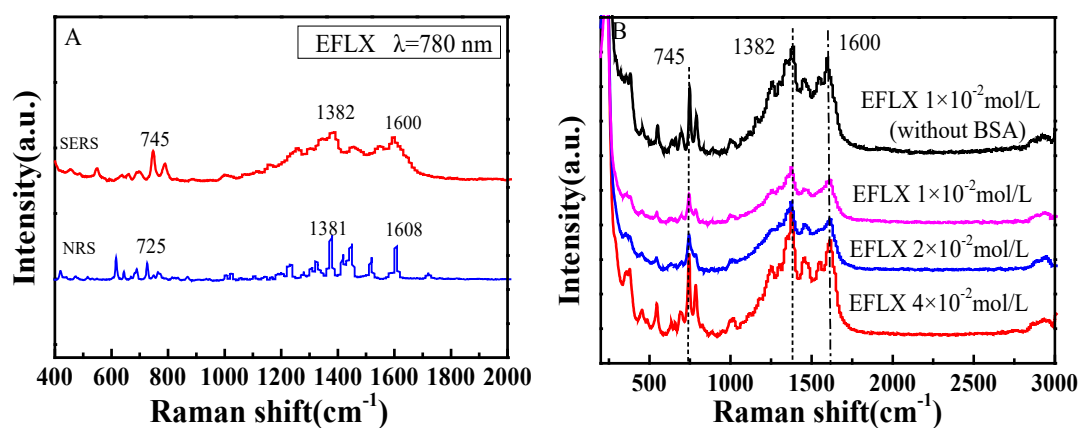


Fig. 3. (A) NR and SERS spectra of EFLX at 780 nm, (B) SERS spectra of EFLX before and after binding with BSA.

3.3. UV-VIS spectroscopy analysis

UV-VIS absorption spectroscopy, has been used to investigate the interaction of drugs with small molecules by monitoring changes of UV-VIS absorption bands of drugs or small molecules. Generally, in the static mechanism, changes in the absorption spectrum are expected due to the formation of a new species (drug-BSA complex)^[22]. Proteins can be detected easily by a UV absorbance detector, because the peptide bonds between amino acids and aromatic side groups in protein molecules absorb UV light at 200-220 nm and 280 nm, respectively. Here, the UV-VIS spectra of different concentrations of EFLX on bovine serum albumin were measured in order to analyse the burst mechanism. As seen from ultraviolet visible emission spectra of EFLX-BSA complexes (Fig.4), an typical absorption peak was formed at 280 nm owing to the $\pi \rightarrow \pi^*$ leap of the indole ring of the Trp residue in BSA. With the addition of EFLX solution to BSA, it was observed that a progressive increase in the ultraviolet intensity, accompanied by a blue shift.

Interactions between EFLX with BSA molecules were investigated and the experimental results probably indicated that the interaction of EFLX to BSA can easily change the conformation of the BSA molecule and it was altered to a more extended state owing to the non-dense hydrophobic substructure (Trp214 residue), which could be in accordance with reported literature^[23]. Consequently, it showed that EFLX has static burst function to BSA, which had been confirmed definitely via the appearance of a new absorption band at 300-350 nm.

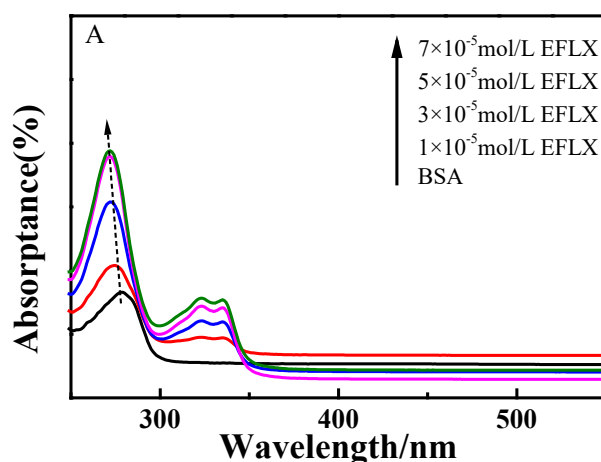


Fig. 4. UV-Vis spectrum of EFLX-BSA interaction.

3.4. Fluorescence spectroscopy analysis

Fluorescence emission spectra of BSA of different concentrations in Tris-HCl buffer (10mM, pH=7.4) were obtained with the excitation wavelength at 295 nm in Fig. 5. BSA exhibited a strong fluorescence emission with a peak at around 345 nm owing to the single tryptophan residue (Trp 213). With increasing concentration of EFLX to BSA, it observed that a progressive decrease in the fluorescence intensity of tryptophan residue was caused by quenching, accompanied by a discolouration shift of the maximum emission. The phenomenon probably indicated that the interaction between EFLX and BSA can lead to the conformation change of BSA, and also confirmed that EFLX binds to BSA to form the ground state complex. This also suggested that the drug affects the microenvironment around the tryptophan residues of bovine serum albumin upon ligand binding, increasing their polarity, as well as affecting the fluorescence intensity.

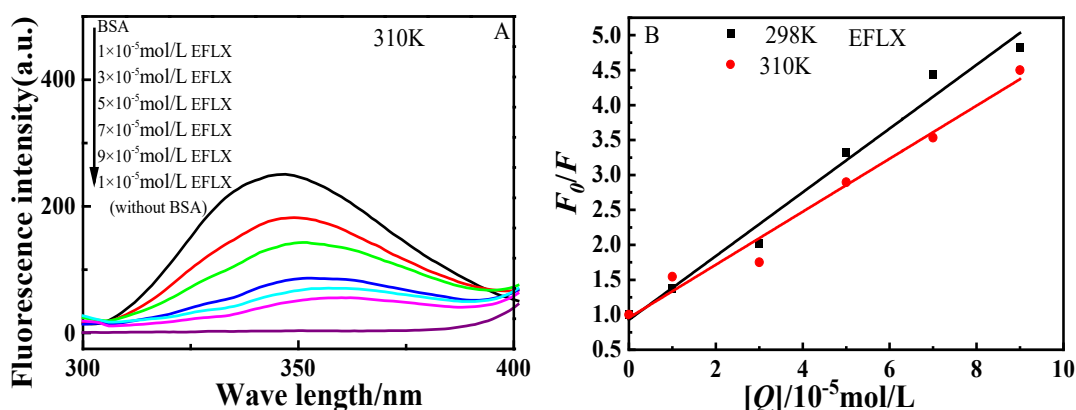


Fig. 5. (A) Effect of EFLX on the fluorescence spectrum of BSA at 310 K, (B) Stern-Volmer plots of EFLX and BSA at different temperatures.

Table 1. Stern-Volmer burst constants for systems at different temperatures.

T/K	Stern-Volmer equation	$K_{sv}/(\text{L}\cdot\text{mol}^{-1})$	$K_q/(\text{L}\cdot\text{mol}^{-1}\cdot\text{s}^{-1})$	R^2
298	$F_0/F=4.56\times 10^4[Q]+0.9282$	4.56×10^4	4.56×10^{12}	0.9909
310	$F_0/F=3.79\times 10^4[Q]+0.9576$	3.79×10^4	3.79×10^{12}	0.9895

Note: R is the linear relative coefficient of $(F_0/F) - [Q]$.

The fluorescence burst mechanism can be easily classified as dynamic burst, static burst and combined burst forms. To elucidate the fluorescence quenching mechanism, the data were analysed using the Stern-Volmer equation as follows^[24]:

$$\frac{F_0}{F} = 1 + K_q\tau_0[Q] = 1 + K_{sv}[Q] \quad (1)$$

F_0 and F are the correct fluorescence intensities of BSA in the absence and presence of the quencher, respectively; τ_0 is the average lifetime of molecular fluorescence with the value of 10^{-8} s; K_{sv} is the Stern-Volmer dynamic quenching constant; K_q is the quenching rate constant of the biomolecule; $[Q]$ is the quencher concentration. According to F_0/F versus $[Q]$, the value of K_q can be obtained (Table 1). The value of K_{sv} is inversely proportional to temperature and K_q is much larger than the maximum scattering collisional burst constant ($2\times 10^{10} \text{ L}/(\text{mol}\cdot\text{s}^{-1})$)^[25]. Hence, this indicates that the fluorescence quenching was not originated by dynamic collision, but it must be caused by a specific interaction between BSA and the complexes, suggesting a static quenching mechanism.

The Lineweaver-Burk equation^[26] usually be used to calculate the binding constant (K_A) and the number of binding sites (n) when a small molecule binded independently to a set of equivalent sites on a large molecule, calculated as equation (2) below:

$$\log[(F_0 - F) / F] = \log K_A + n \log [Q] \quad (2)$$

The $\log(F_0 - F)/F$ and $\log[Q]$ curves were plotted to analysis the binding constants, number of binding sites and forces between EFLX and BSA(Fig.6), and the calculated records were shown in Table 2.The corresponding results depicted that straight lines had a good linearity relationship with perfect correlation coefficients ($R^2 > 0.95$), and the number of binding sites was calculated ($n \approx 1$), indicating that there was only one binding site for EFLX and BSA. In addition, the picture revealed that the binding constants of EFLX-BSA increased and the calculated binding constant of EFLX-BSA was 10^4 . Consequently, it displayed that the binding between EFLX and BSA was a heat-absorbing reaction and the binding affinity was moderate.

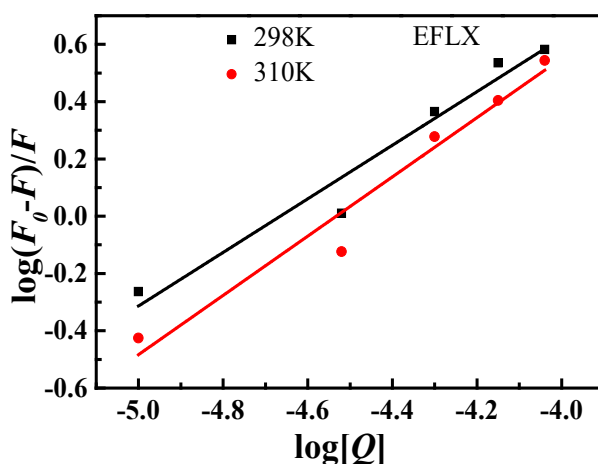


Fig. 6. Double logarithmic plot of fluorescence burst of BSA by EFLX.

Table 2. Binding constants (K_A) and number of binding sites (n) for the interaction of enrofloxacin with BSA.

T/K	Lineweaver-Burk equation	$K_A/(\text{L} \cdot \text{mol}^{-1})$	n	R^2
298	$\text{Log}(F_0 - F)/F = 0.9355 \log[Q] + 4.364$	2.312×10^4	0.9355	0.9791
310	$\text{Log}(F_0 - F)/F = 1.0343 \log[Q] + 4.688$	4.879×10^4	1.034	0.9805

Note: R is the correlation coefficient of the $\log[(F_0 - F) / F] - \log[Q]$ curve

Rose have reported that the various types of forces of interaction that act between any compound and the protein could be indicated by the sign and magnitude of the thermodynamic parameters as follows^[27]: (1) the positive values for both ΔH and ΔS correspond to the involvement of hydrophobic forces in protein binding, (2) the negative values for both ΔH and ΔS correspond to van der Waals and hydrogen bonding interactions, and (3) the negative value of ΔH and the positive value of ΔS indicate electrostatic interaction. The thermodynamic parameters were calculated according to the van der Hove equation:

$$\ln K_A = -\frac{\Delta H}{RT} + \frac{\Delta S}{R} \quad (3)$$

$$\Delta G = \Delta H - T\Delta S = -RT \ln K_A \quad (4)$$

The thermodynamic parameters $\Delta H > 0$, and $\Delta S > 0$ for EFLX and BSA obtained according to Eq. indicated that the main forces of EFLX and BSA are hydrophobic.

To determine the favorable binding sites of EFLX on BSA, site-competitive labelling experiments with the well-known site markers were employed using phenylbutazone, ibuprofen, and digitoxin as a site probe for site I, site II, and site III, respectively^[28].

K'_A was the binding constant of the system in the presence of the labelling reagent. The binding constant K'_A and the rate of the binding constant (φ) of the system were calculated from equation (2) and equation (5)^[29]:

$$\varphi = (K'_A - K_A) / K_A \quad (5)$$

As seen from the corresponding calculations which were given in Figure 7 and Table 3. The binding of the enrofloxacin to the bovine serum albumin molecule was affected by the presence of an additional drug ligand, which was reflected by the reduced binding constant of the EFLX-BSA-DRUG system. The presence of phenylbutazone in the EFLX-BSA system strongly influenced the quenching behavior and the binding constant. Hence, this suggested that EFLX was predominantly substituted by phenylbutazone, and competed with Site I of BSA.

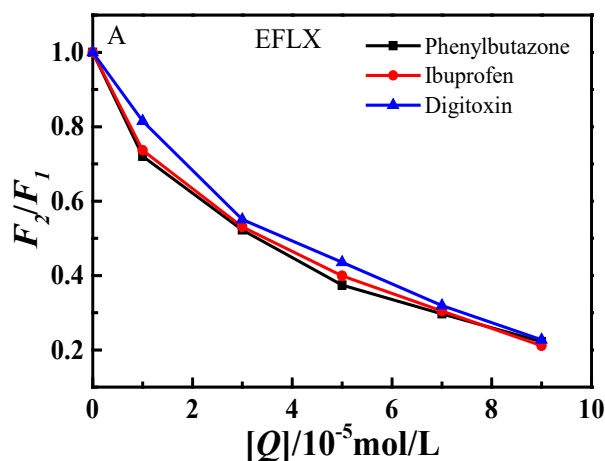


Fig. 7. Effect of three site-specific markers on the fluorescence intensity of the EFLX-BSA system.

Table 3. Binding constants K'_A and the number of binding sites in the system in the absence and presence of the 298k locus marker.

Site marker	$K'_A/(\text{L}\cdot\text{mol}^{-1})$	n	R^2	$\varphi\%$
Blank	2.31×10^4	0.9355	0.9791	
Phenylbutazone	7.72×10^3	0.8124	0.9857	-66.57%
Ibuprofen	1.89×10^4	0.9243	0.9836	18.35%
Digitoxin	3.10×10^4	0.9721	0.9898	-29.74%

4. Conclusion

In this paper, the interactions of enrofloxacin with BSA was characterized by means of Raman, SERS, ultraviolet as well as fluorescence spectroscopy. From these experiments, the observed changes in SERS intensity of enrofloxacin with BSA explained the assumption that these moleculars were absorbed on the substrate surface. In addition, the ultraviolet and fluorescence analysis unveiled that EFLX can statically burst the fluorescence of BSA with a binding constant of 10^4 , and a hydrophobic effect between enrofloxacin and BSA. According to the site-competitive labelling experiments, it indicated that the the binding site of EFLX to BSA was at site I.

Acknowledgements

This research was funded through a grant from the Hebei Natural Science Foundation, contract No.H2022209066.

References

- [1] J. Seetharamappa , B. Kamat, Pharm. Biomed. Anal, 39(10), 104 (2005);
- [2] A. Sulkowska , 14(5), 227 (2002); <https://doi.org/10.1023/A:1015879627234>
- [3] Y. Lou, K. Zhou, D. Q. Pan, Photochem. Photobiol. B,17(3), 167 (2017).
- [4] J. Guan , X. Yan , Y. J. Zhao, Spectrochim Acta A, 12(2), 202 (2018); <https://doi.org/10.1016/j.saa.2018.04.070>
- [5] S. Ashoka , J. Seetharamappa , B. Kandagal, Journal of Luminescence, 19(1), 179 (2006); <https://doi.org/10.1016/j.jlumin.2005.12.001>
- [6] P. Bourassa, C. D. Kanakis, P. Tarantilis, Phys. Chem. B, 6(2), 114 (2010); <https://doi.org/10.1021/jp9115996>
- [7] S. Schlucker, Angew Chem, 22(4), 53 (2014).
- [8] D. Karthigeyan, S. Siddhanta, A. H. Kishore, Proc Natl Acad Sci, 13(8), 111 (2014); <https://doi.org/10.1073/pnas.1402695111>
- [9] R. Ban, Y. Yu, M. Zhang, ACS Applied Materials & Interfaces, 9(15), 76 (2017); <https://doi.org/10.1021/acsami.6b15396>

- [10] Y. Ma, D. Sikdar, A. Fedosyuk, *ACS nano*, 14(1), 328 (2020);
<https://doi.org/10.1021/acsnano.9b05257>
- [11] W. Lian, Y. Liu, H. Yang, *Spectrochimica Acta Part A Molecular and Biomolecular Spectroscopy*, 20(7), 307 (2018); <https://doi.org/10.1016/j.saa.2018.09.034>
- [12] G.V. Naik, V. M. Shalaev, A. Boltasseva, *Adv. Mater*, 18(2), 326 (2013).
- [13] U. Guler, V. M. Shalaev, A. Boltasseva, *Mater. Today*, 11(5), 227 (2015);
<https://doi.org/10.1016/j.mattod.2014.10.039>
- [14] P. Patsalas, N. Kalfagiannis, S. Kassavetis, *Materials*, 27 (8), 312 (2015);
<https://doi.org/10.3390/ma8063128>
- [15] I. Lorite , A. Serrano , A. Schwartzberg, *Thin Solid Films*, 5 (1), 144 (2013);
<https://doi.org/10.1016/j.tsf.2013.01.024>
- [16] J. H. Zhao, J. Lin, H.Y. Wei, *Opt. Mater*, 10(4), 67 (2015).
- [17] X. Li, P. X.Wang, Y. Sun, *ACS Appl Mater Interfaces*, 21(7), 71 (2015);
<https://doi.org/10.1021/acsami.5b02666>
- [18] J. S. Suh, M. Moskovits, *Journal of the American Chemical Society*, 108(16), 47 (2016).
- [19] Y. F. Zhang, K. L. Zhou, D. Q. Lou, *Journal of Biomolecular Structure & Dynamics*, 35(12),36 (2017).
- [20] W. R. Ware, *Journal of Physical Chemistry*, 66(3), 45 (1992).
- [21] L. Vergani, G. Mascetti, P. Gavazzo, *ThermochimicaActa*, 294(2), 193 (1997);
[https://doi.org/10.1016/S0040-6031\(96\)03123-1](https://doi.org/10.1016/S0040-6031(96)03123-1)
- [22] H. Y. Wei, M. M. Wu, Z. L. Dong, *Journal of Raman Spectroscopy*, 48(4), 57 (2017);
<https://doi.org/10.1002/jrs.5080>
- [23] X. Peng, X. C. Wang, W. Qi, *Food Chemistry*, 196(13),178 (2016);
<https://doi.org/10.1016/j.foodchem.2015.06.109>
- [24]A. Naseri, S. Hosseini, F. Rasoulzadeh, *Journal of Luminescence*, 157(25), 104 (2016);
<https://doi.org/10.1016/j.jlumin.2014.08.031>
- [25] Y. Zhang, Y. Huang, F. Zhai, *Food Chemistry*, 135(2), 84 (2012);
<https://doi.org/10.1016/j.foodchem.2012.04.082>
- [26] P. D. Ross, S. Subramanian, *Biochemistry*, 20(11), 30 (1991).
- [27] D. Silva, C. M. Cortez, S. Louro, *Spectrochimica Acta Part A Molecular & Biomolecular Spectroscopy*, 60(5), 121 (2004); <https://doi.org/10.1016/j.saa.2003.08.003>
- [28] K. Y. Hong, C. D. Albuquerque, R. J. Poppi, *Analytica Chimica Acta*, 98(2),148 (2017);
<https://doi.org/10.1016/j.aca.2017.05.025>
- [29] I. Sjoholm, B. Ekman, A. Kober, 16(3), 76 (1999).
- [30] B. S. Liu, J. Wang, C. L. Xue, *Monatshefte Fur Chemie*, 143(3), 40 (2012);
<https://doi.org/10.1007/s00706-011-0593-4>